ISSN (Print) 1226-1750
ISSN (Online) 2233-6656
Journal of Magnetics 27(3), 263-271 (2022) https://doi.org/10.4283/JMAG.2022.27.3.263

Two-dimensional Harmonic Modelling for Electro-magnetic Solution in Cartesian Coordinates

Yunlu Du[1]*, Baocheng Guo[2], Z. Djelloul-khedda[3], Fei Peng[1], and Yunkai Huang[1]

[1]*School of Electrical Engineering, Southeast University, Nanjing 210096, China*
[2]*School of Electrical and Automation Engineering, Nanjing Normal University, 210023, China*
[3]*1LESI Laboratory, Univ. Djilali Bounaama Khemis Miliana, Road of Theniet El-had, Khemis Miliana, 44225, Algeria*

(Received 5 April 2022, Received in final form 15 July 2022, Accepted 21 July 2022)

This paper first presents a general two-dimension (2D) harmonic analytical solution for the magnetic field of electric machines in the Cartesian coordinates. In this solution, the relative permeance is directly considered in Laplace and Poisson's equations, and the particular solutions in Cartesian coordinates are solved. By applying the complex Fourier separation method, with the boundary and interface conditions, the magnetic field in the inhomogeneous region is solved from system equations. Numerical examples validate the presented method and the obtained results have a satisfactory agreement with the finite element analysis. The proposed model in this paper has a significant value for modelling electric machines, such as linear permanent magnet (PM) machines and axial flux PM machines.

Keywords : harmonic model, orthotropic material, analytical solution, magnetic field

1. Introduction

Nowadays, for the sustainable development of the environment, there is a critical need for "electrification or "more electric in industrial applications [1]. Therefore, electrical machines (EE) play a key role in the foreseeable future.

Several approaches are utilized to design electric machines. The finite element model (FEM) is the most commonly used due to its high accuracy and friendly Human-machine interface [2-4]. However, the time cost of FEM simulation is often counted by hours or even days when the 3D geometry is complex, which is the case for axial flux PM machines [5, 6]. Designers have to make a trade-off between accuracy and computational time on the modelling. An alternative method is analytical modelling (AM), which is a powerful tool to calculate the magnetic field of the EE [7]. What's more, AM can provide valuable insight into the parameters in the equations. Therefore, it is widely used in the EE initial design and optimization stages.

Until now, several analytical models for electromagnetic field calculation have been developed and proposed, for example, Schwarz-Christoffel (SC) mapping and sub-domain model (SDM). It has been a challenge to model the magnetic nonlinearity in EE accurately using analytical methods since the iron permeability change significantly as the magnetic core saturates. In [8, 9], the relative permanence in the air gap could be obtained by SC mapping, thus, the slot effect is considered. In [10, 11], the SDM is used to obtain the general expression of each domain by the separation of variables. However, most of the AMs are developed based on the assumption that iron materials have infinite permeance, thus the saturation effect in a ferromagnetic material is ignored. This assumption causes calculation errors. To solve this problem, two approaches are proposed. One is the elementary SDM proposed by Dubas, which divides the motor into multiple solution domains, and solves the partial differential equations of each domain [12]. The other method is harmonic modelling (HM) developed by Sprangers, which gives the general solution of the EE in 2D polar coordinates and has been widely used [13]. Different from elementary SDM, the HM technology considers the permeance of the iron part and embeds it into the complex general solutions. In [14], Z.Djelloul considers the local magnetic saturation in the iron parts and calculates the electromagnetic performance of the switch reluctance machine. Further

*Corresponding author: Tel: +86-15855153683
Fax: +86-25-83792260, e-mail: duyl@seu.edu.cn

work is carried out on the prediction of iron-core loss in PM machines [15]. For more complex electromagnetic structures, such as coaxial magnetic gears, the HM also has achieved good accuracy [16]. From the literature survey, we can learn that the HM can well consider the non-linear properties of the ferromagnetic materials. It is worthy to point out that all previous studies are focused on the radial flux motors in the polar coordinates system. With regards to the axial flux PM and linear PM machines, which are modeled in Cartesian coordinates, there are no solutions.

In this paper, the first analytical solution based on the HM approach for the 2D electromagnetic in Cartesian coordinates is developed and presented. The proposed model divides nonlinear ferromagnetic materials into several parts and considers the influence of material nonlinearity and local saturation through the iterative algorithm. The correctness of the proposed model is verified by comparing the HM and FEM results of two numerical examples. Moreover, the proposed model is an effective tool and has significant value for the design and optimization of other types of electromagnetic devices in the Cartesian coordinates system.

The paper is organized as follows: Section II derives the general form of the harmonic model in the 2D Cartesian coordinates system. In Section III, two numerical examples are introduced to verify the HM, and the solutions of partial differential equations in each subdomain are given. In Section IV, the iterative algorithm considering the nonlinearity of ferromagnetic materials is introduced. The results from the proposed approach and FEM are compared in Section VI. The conclusions of the research are reached at the end of the paper.

2. Harmonic Subdomain Model in Cartesian Coordinates

According to Gauss's law, the magnetic flux density vector B is divergence-free, i.e., $\nabla \cdot B = 0$. In addition, in the absence of any current, according to Ampere's law of magnetism, the magnetic field intensity vector H is curl-free, i.e., $\nabla \times H = 0$, or $\nabla \times H = J$ under the current situation [17]. The constitutive relation between B and H, given by

$$B = \mu_0 \mu_{rec} H + \mu_0 M \tag{1}$$

where M is the magnetization vector, μ_0 is the free space permeability, and μ_{rec} is the relative permeability of the PM material. Substituting (1) into Ampere's law yields

$$\nabla \times B = \mu_0 \nabla \times M \tag{2}$$

Using the magnetic potential vector,

$$B = \nabla \times A \tag{3}$$

Substituting (1) into (2) and choosing Coulomb gauge $\nabla \cdot A = 0$, Poisson's equation is obtained as

$$-\nabla^2 A = \mu_0 J + \mu_0 (\nabla \times M) \tag{4}$$

The magnetic field equation for the considered Cartesian coordinates system results in

$$\frac{\partial^2 A}{\partial x^2} + \frac{\partial^2 A}{\partial z^2} = -\mu_0 \left(\frac{\partial M_z}{\partial x} - \frac{\partial M_x}{\partial z} \right) - \mu_0 J \tag{5}$$

where M_z and M_x are the normal and tangential components of M, respectively; J is the current density.

In the Cartesian coordinates, we define the calculation region length L in x-direction equals $2\pi R_m$, then, the length x can be replaced by angle θ by using the formula x/R_m, as shown in Fig. 1(b) [11].

Then, (5) can be rewritten as [18]

$$\frac{\partial^2 A}{\partial z^2} + \frac{1}{R_m^2} \frac{\partial^2 A}{\partial \theta^2} = -\mu_0 \left(\frac{\partial M_z}{\partial x} - \frac{\partial M_x}{\partial z} \right) - \mu_0 J \tag{6}$$

For the magnetic vector potential A, the complex Fourier series representation is given by [13]

$$A(z,\theta) = \sum_{n=-\infty}^{\infty} \hat{A}_n(z) e^{-jn\theta} \tag{7}$$

where n represents the harmonic ordinal number.

Thus, the relations between the Fourier series coefficients of B in θ- and z-directions with that of the magnetic vector potential A in z-direction A_z can be expressed as [15]:

$$B_z = \frac{1}{R_m} \frac{\partial A}{\partial \theta} = -j \frac{1}{R_m} K_\theta A, \text{ and } B_\theta = -\frac{\partial A}{\partial z} \tag{8}$$

where B_z and B_θ are the normal and tangential components of magnetic flux density, respectively. K_θ is the diagonal matrix of harmonic order n, given by

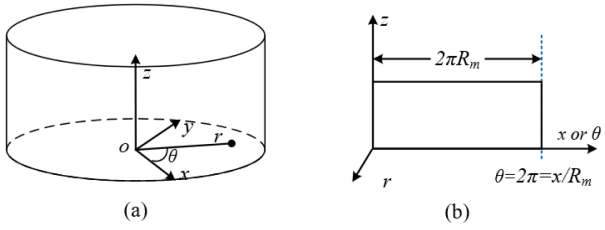

Fig. 1. 2D Cartesian coordinates model. (a) A cylinder in the Cartesian coordinates system, (b) Definition of a point (z, θ) with respect to the cartesian coordinates system (z, x).

$$K_\theta = \begin{bmatrix} -N_{sh} & \cdots & 0 \\ \vdots & \ddots & \vdots \\ 0 & \cdots & N_{sh} \end{bmatrix} \tag{9}$$

where N_{sh} represents the highest spatial harmonic taken into account in the magnetic field solution.

Then, substituting (8) into (1), the expression for magnetic field strength in normal direction H_z and tangential direction H_θ are obtained as

$$H_z = -j\frac{1}{R_m}\mu_{c,z}^{-1}K_\theta A_z, \; and \; H_\theta = -\mu_{c,\theta}^{-1}\frac{\partial A_z}{\partial z} \tag{10}$$

where $\mu_{c,z}$ and $\mu_{c,\theta}$ represent the permeability convolution matrices for the normal and the circumferential component respectively.

Thus, $\nabla \times H = J$ can be rewritten as

$$\frac{\partial H_\theta}{\partial z} + j\frac{1}{R_m}K_\theta H_z = J_z \tag{11}$$

After substituting (10) into (11), the magnetic field equation for the inhomogeneous region is obtained as

$$\frac{\partial^2 A}{\partial z^2} - \frac{1}{R_m^2}VA_z = -\mu_0\frac{1}{R_m}M_\theta - j\mu_0\frac{1}{R_m}SM_z - \mu_{c,\theta}J \tag{12}$$

where $V = \mu_{c,\theta}K_\theta\mu_{c,z}^{-1}K_\theta$, and $S = \mu_{c,\theta}K_\theta\mu_{c,z}^{-1}$.

Thus, A can be solved using the separated variables method, as

$$A = a_n e^{\frac{z}{R_m}V} + b_n e^{-\frac{z}{R_m}V} + R_m^2F_1 + R_mF_2 \tag{13}$$

where

$$F_1 = -j\mu_0 V_I^{-2}\mu_{c,\theta}^I K_\theta \mu_{c,z}^{-1}M_z \tag{14}$$

$$F_2 = V^{-1}\mu_{c,\theta}J_z \tag{15}$$

3. Comprehensive Numerical Examples

To verify the proposed 2D harmonic model, the obtained formulations are implemented for two slotted benchmark topologies, as shown in Fig. 2. The parameters of the benchmark topology are given in Table 1. To simplify the analysis, the nonlinearity of the backplates of the two models is not considered ($\mu_r = \infty$), while the nonlinearity of the rest of the ferromagnetic materials is discussed in detail in section III.

Model A is divided into two calculation regions, namely, the air-gap region (region I) and the stator-winding region (region II), while model B is divided into three calculation regions, namely, the stator-winding region (region I), the air-gap region (region II), and the nonlinear region of ferromagnetic materials (region III). The magnetic field is generated by applying current to the windings. The analytical calculation results of the magnetic field components in the air-gap region are compared with the FEM to verify the proposed 2D harmonic model.

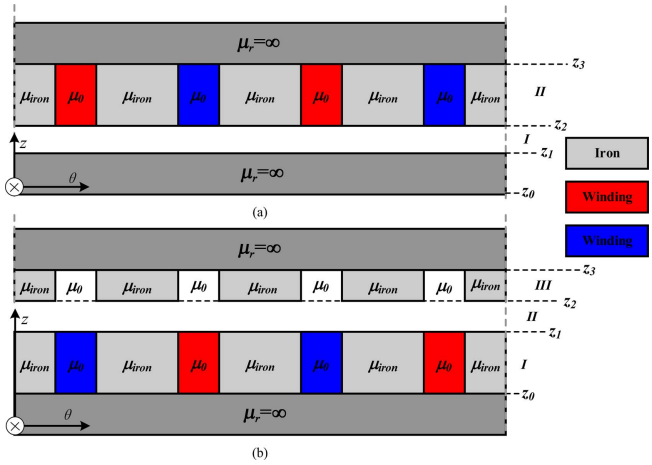

Fig. 2. (Color online) Benchmark topologies are used for the validation of the presented model. (a) model A, (b) model B.

Table 1. Geometric parameters of model A and model B.

Model	z_0/mm	z_1/mm	z_2/mm	z_3/mm
A	0	10	16.7	39.6
B	0	22.9	27.6	37.6

The angular position of i-th stator slot opening is defined by

$$\alpha_i = \frac{2\pi}{Q_s}i - \frac{\pi}{Q_s}, i = 1,2,\cdots,Q_s \tag{16}$$

where Q_s is the number of stator slots.

The current density J and the complex Fourier series expansion $J_z(\theta)$ are given by

$$J = J_z(\theta)e_z \tag{17}$$

$$J_z(\theta) = \sum_{n=-\infty}^{n=\infty}\hat{J}_{z,n}e^{-jn\theta} \tag{18}$$

The complex Fourier coefficients of $\hat{J}_{z,n}$ can be obtained by

$$\hat{J}_{z,n} = \frac{1}{2\pi jn}\sum_{i=1}^{Q_s}\left[J_{i,1}\left(e^{jnd}-1\right)e^{-jn\frac{\theta_{ss}}{2}} + J_{i,2}\left(1-e^{-jnd}\right)e^{jn\frac{\theta_{ss}}{2}}\right]e^{jn\alpha_i} \tag{19}$$

where θ_{ss} and d are stator slots width and windings width, respectively.

The current densities of the double-layer windings are

defined as

$$J_{i,1} = \frac{N_c}{S} C_1^T \left[i_A, i_B, i_C \right] \tag{20}$$

$$J_{i,2} = \frac{N_c}{S} C_2^T \left[i_A, i_B, i_C \right] \tag{21}$$

where N_c is the conductor number of the slot coil, [i_A, i_B, i_C] are the armature currents, S is the surface of the stator slot coil, C_1^T and C_2^T are the transpose of the connecting matrix between the three-phases current and the stator slots, which represent the distribution of stator windings in the slots.

For the sake of clarity of the general solutions in the different domains, the following notation is adopted in this paper

$$P_\omega \left(\alpha, \beta, \gamma \right) = R_m \left(\frac{e^{\frac{\beta}{\alpha}}}{e^{\frac{\gamma}{\alpha}}} \right)^\omega \tag{22}$$

The solution of model A for each region is formulated as follows

$$A_I \mid_z = a_I P_{V_I} \left(R_m, z, z_2 \right) + b_I P_{V_I} \left(R_m, z_1, z \right) \tag{23}$$

$$A_{II} \mid_z = a_{II} P_{V_{II}} \left(R_m, z, z_3 \right) + b_{II} P_{V_{II}} \left(R_m, z_2, z \right) \tag{24}$$

and for model B

$$A_I \mid_z = a_I P_{V_I} \left(R_m, z, z_1 \right) + b_I P_{V_I} \left(R_m, z_0, z \right) + R_m^2 F_2 \tag{25}$$

$$A_{II} \mid_z = a_{II} P_{V_{II}} \left(R_m, z, z_2 \right) + b_{II} P_{V_{II}} \left(R_m, z_1, z \right) \tag{26}$$

$$A_{III} \mid_z = a_{III} P_{V_{III}} \left(R_m, z, z_3 \right) + b_{III} P_{V_{III}} \left(R_m, z_2, z \right) \tag{27}$$

The unknown coefficient matrices, **a** and **b**, in (23)-(24) and (25)-(27), are usually obtained from the boundary conditions and interface conditions of the magnetic field.

For model A, boundary conditions between two adjacent media are

$$A_I \mid_{z=z_2} \left(z, \theta \right) - A_{II} \mid_{z=z_2} \left(z, \theta \right) = 0 \tag{28}$$

$$H_\theta^I \mid_{z=z_2} \left(z, \theta \right) - H_\theta^{II} \mid_{z=z_2} \left(z, \theta \right) = 0 \tag{29}$$

Furthermore, at the outer boundary of the region I and region II, an interface with infinitely relative permeability material is assumed, therefore

$$H_\theta^I \mid_{z=z_1} \left(z, \theta \right) = 0 \tag{30}$$

$$H_\theta^{II} \mid_{z=z_3} \left(z, \theta \right) = 0 \tag{31}$$

According to the same principle, for model B, boundary conditions are

$$A_I \mid_{z=z_1} \left(z, \theta \right) - A_{II} \mid_{z=z_1} \left(z, \theta \right) = 0 \tag{32}$$

$$H_\theta^I \mid_{z=z_1} \left(z, \theta \right) - H_\theta^{II} \mid_{z=z_1} \left(z, \theta \right) = 0 \tag{33}$$

$$A_{II} \mid_{z=z_2} \left(z, \theta \right) - A_{III} \mid_{z=z_2} \left(z, \theta \right) = 0 \tag{34}$$

$$H_\theta^{II} \mid_{z=z_2} \left(z, \theta \right) - H_\theta^{III} \mid_{z=z_2} \left(z, \theta \right) = 0 \tag{35}$$

$$H_\theta^I \mid_{z=z_0} \left(z, \theta \right) = 0 \tag{36}$$

$$H_\theta^{III} \mid_{z=z_3} \left(z, \theta \right) = 0 \tag{37}$$

Finally, all boundary condition equations are collected and written in matrix form as

$$UF = Y \tag{38}$$

where U, F, and Y represent the unknown coefficients, the coefficient factors, and the constant values in the boundary condition equations, respectively.

According to the above analysis, the magnetic vector potential A_k of each region can be obtained. Then, B_z and B_θ of each region can be deduced from A_k.

$$B_z^k \mid_z = -j \frac{1}{R_m} K_\theta A_k, \; B_\theta^k \mid_z = -\frac{\partial A_k}{\partial z} \tag{39}$$

4. The Nonlinearity of Ferromagnetic Materials

The harmonic subdomain model proposed in this paper can consider the nonlinear effects of ferromagnetic materials. As shown in Fig. 3, the permeability distribution can be expressed as [14]

$$\mu(\theta) = \begin{cases} \mu_{iron} & \left[\gamma_k + \frac{\theta_2}{2}, \gamma_k + \theta_1 + \frac{\theta_2}{2} \right] \\ \mu_0 & \left[\gamma_k + \theta_1 + \frac{\theta_2}{2}, \gamma_k + \theta_1 + \frac{3\theta_2}{2} \right] \end{cases} \tag{40}$$

However, $\mu(\theta)$ can also be expressed as a complex Fourier series form as

$$\mu(\theta) = \sum_{n=-\infty}^{\infty} \hat{\mu}_n e^{-jn\theta} \tag{41}$$

$$\mu^{rec}(\theta) = \sum_{n=-\infty}^{\infty} \hat{\mu}_n^{rec} e^{-jn\theta} \tag{42}$$

The coefficient $\hat{\mu}_n$ can be obtained by

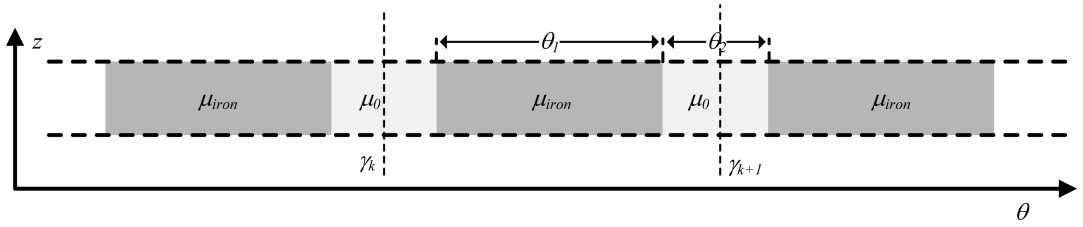

Fig. 3. Permeability distribution of a calculation region.

$$\hat{\mu}_n = \begin{cases} \sum_{k=1}^{Q} \frac{1}{2\pi jn}\left[\mu_{iron} e^{-jn\frac{\theta_2}{2}}\left(1-e^{-jn\theta_1}\right)\right. \\ \left. +2j\mu_0 \sin\left(\frac{n\theta_2}{2}\right)\right] e^{jn\gamma_k} & n \neq 0 \\ \sum_{i=1}^{Q} \frac{1}{2\pi}\left(\mu_{iron}\theta_1 + \mu_0\theta_2\right) & n = 0 \end{cases} \tag{43}$$

To calculate $\hat{\mu}_n^{rec}$, we replace $\{\mu_{iron}, \mu_0\}$ by $\{1/\mu_{iron}, 1/\mu_0\}$ in (43).

The normal and tangential relative magnetic permeability matrices $\mu_{c,z}$, and $\mu_{c,\theta}$ are obtained by

$$\mu_{c,z} = \begin{bmatrix} \hat{\mu}_0 & \cdots & \hat{\mu}_{-2N} \\ \vdots & \ddots & \vdots \\ \hat{\mu}_{2N} & \cdots & \hat{\mu}_0 \end{bmatrix}, \mu_{c,\theta} = \begin{bmatrix} \hat{\mu}_0^{rec} & \cdots & \hat{\mu}_{-2N}^{rec} \\ \vdots & \ddots & \vdots \\ \hat{\mu}_{2N}^{rec} & \cdots & \hat{\mu}_0^{rec} \end{bmatrix}^{-1} \tag{44}$$

According to the magnetic field partial differential equation, it is can be seen that the relative permeability of ferromagnetic materials has been embedded into the solution of the static magnetic field. If the region is divided more precisely along with the normal and tangential directions, as shown in Fig. 4, the influence of the nonlinearity of ferromagnetic materials can be well considered through the iterative algorithm. On the other hand, as the calculation area increases, the calculation time will also increase. Therefore, the division of the nonlinear material calculation area is the compromise between calculation accuracy and calculation time.

Fig. 5(a) is the *B-H* curve of commonly used soft-magnetic materials, according to (1), the μ-*B* curve can be obtained as shown in Fig. 5(b). The μ-*B* function for the iterative calculation can be obtained by fitting the original data [19]. When the ferromagnetic material is saturated, it can be found that the fitting data are in good agreement with the original data.

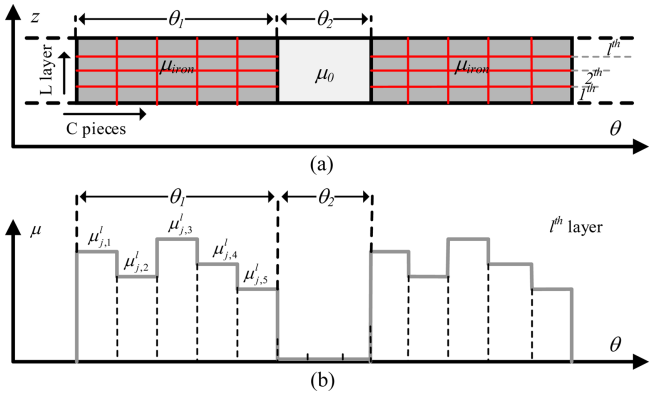

Fig. 4. (Color online) The nonlinearity of ferromagnetic material. (a) Multilayer division of the region, (b) Permeability distribution of *l*th region layer.

Fig. 6 shows the iterative calculation flowchart. First, the relative permeability of each soft-magnetic material is set to the maximum value (μ_r=8000), and then the harmonic coefficient matrix is solved to obtain the magnetic flux density of each calculation area. The relative permeability of the corresponding calculation area is obtained by the μ-*B* curve. Then, the relative permeability of each calculation area is updated until the convergence requirement is met.

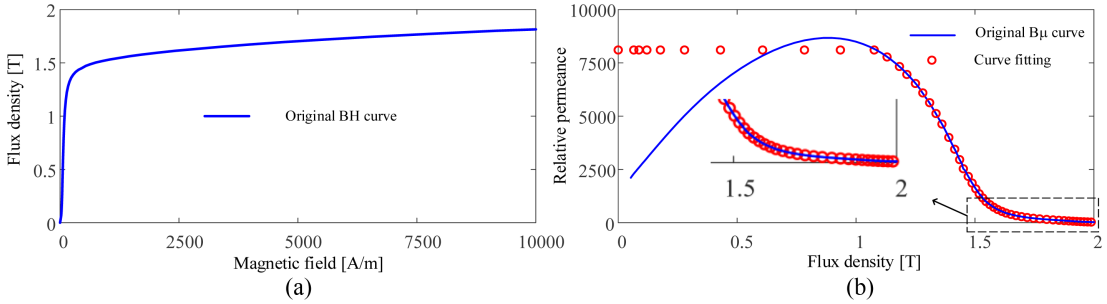

Fig. 5. (Color online) Magnetic characteristics of the soft-magnetic material. (a) *B-H* curve, (b) μ-*B* curve.

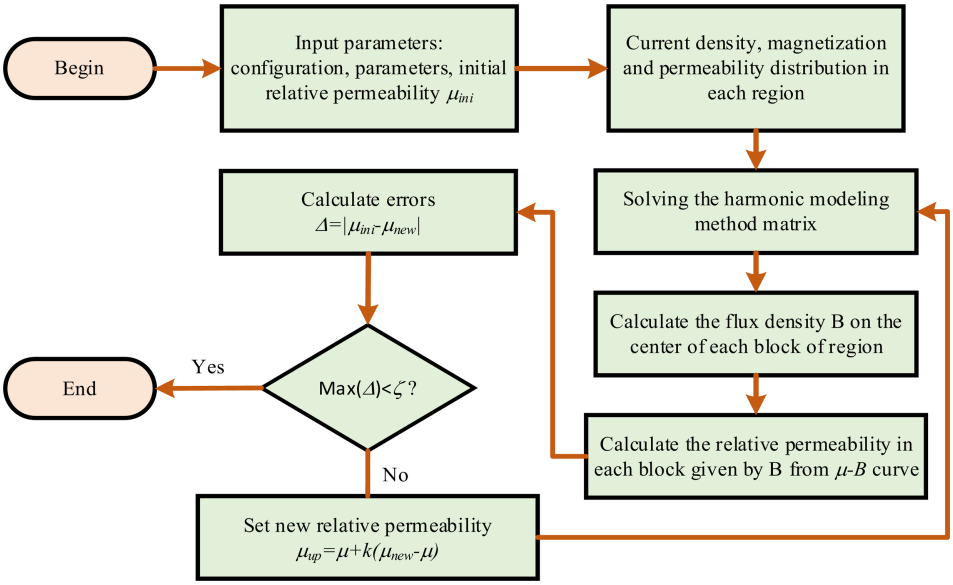

Fig. 6. (Color online) Calculation iteration process flowchart.

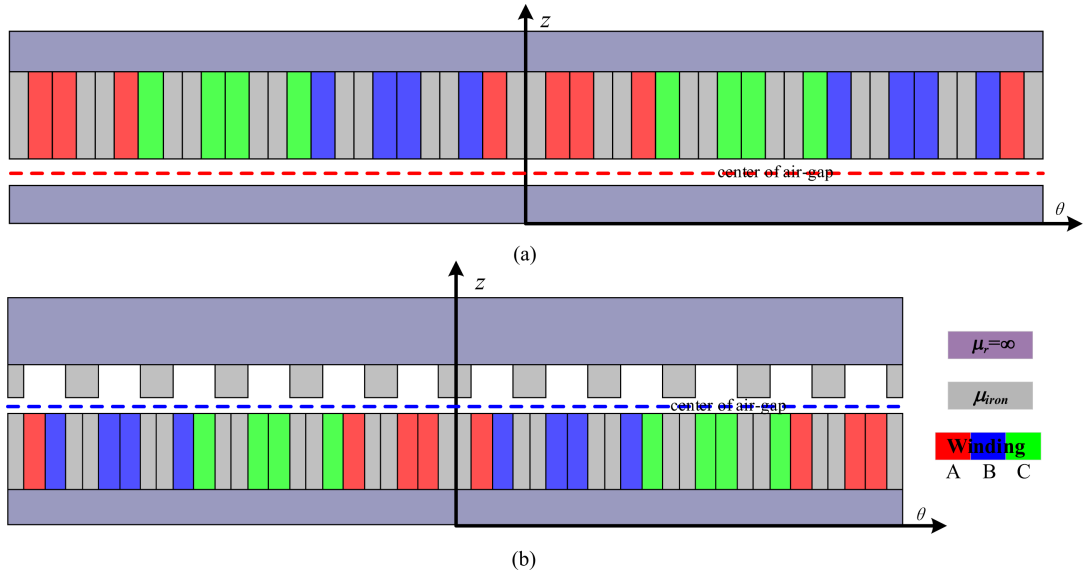

Fig. 7. (Color online) 2D FEM. (a) Model A, (b) Model B.

5. FEM Validation

According to the parameters of Table 1, 2D FEM of Models A and B are established, as shown in Fig. 7. To simplify the analysis model, the relative permeability of yoke ($\mu_r=\infty$) is not considered, and the nonlinearity of tooth ($\mu=\mu_{iron}$) material is only considered.

The load current at a certain time is i_a = 0 A, i_b = 6 A, and i_c = −6 A. The comparison of the normal and tangential components of the flux density at the air-gap center of Model A and B is shown in Fig. 8 and 9. Furthermore, the harmonic spectrum of normal and tangential components is compared. It can be seen from the waveform that the analytical calculation model is in good agreement with the FEM. From the comparison, the harmonic values of the proposed model are close to those of the FEM.

The calculations are carried out for three different values of the relative permeabilities of the studied models (viz., 50, 100, and 1000), and compared to the FEM. The comparison of the air-gap flux density components are shown in Fig. 10 and Fig. 11. It can be found that the analytical model and the FEM are in good agreement under three different relative permeabilities. The proposed model can well consider the saturation effect (viz., the relative permeability is 50).

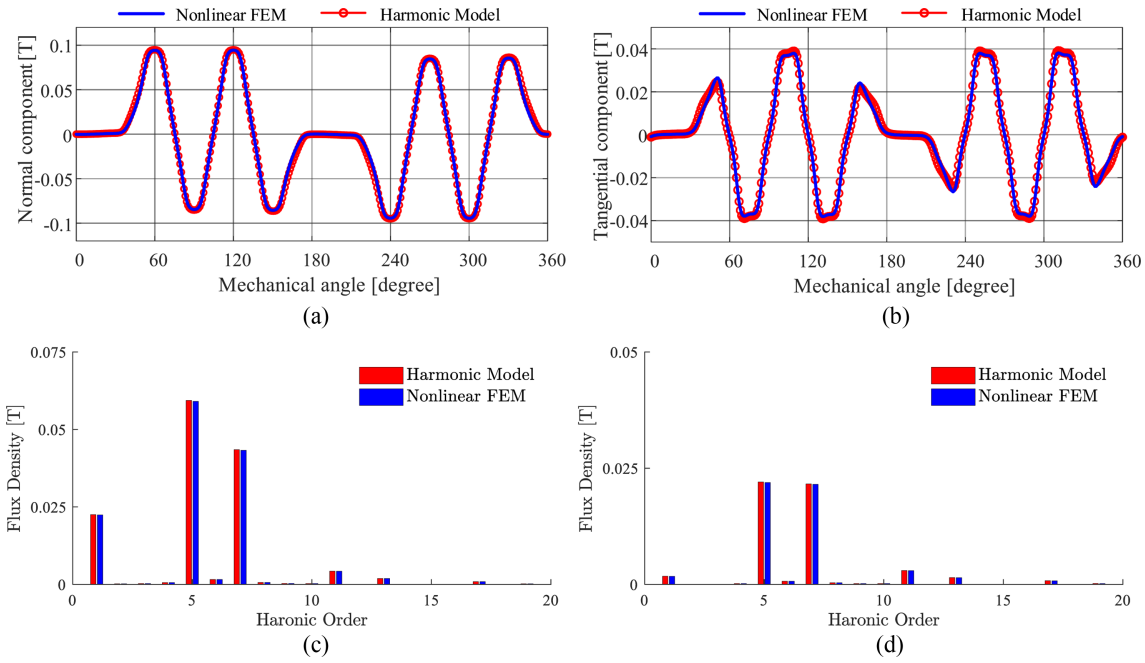

Fig. 8. (Color online) Magnetic flux density distribution in the center of the air-gap of Model A. (a) Comparison of the normal component, (b) Comparison of the tangential component, (c) Harmonic spectrum of the normal component, (d) Harmonic spectrum of the tangential component.

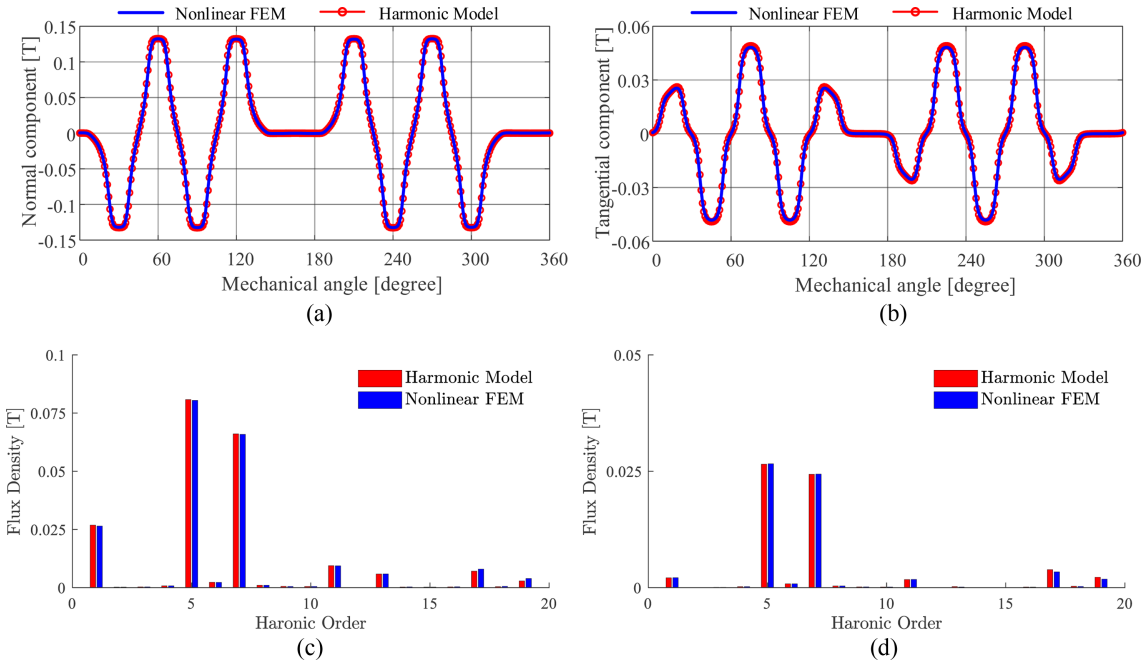

Fig. 9. (Color online) Magnetic flux density distribution in the center of the air-gap of Model B. (a) Comparison of the normal component, (b) Comparison of the tangential component, (c) Harmonic spectrum of the normal component, (d) Harmonic spectrum of the tangential component.

In the harmonic subdomain model proposed in this paper, the selection of harmonic numbers not only affects the calculation accuracy but also affects the calculation time. The root-mean-square (RMS) error is used to evaluate the calculation accuracy of the analytical model proposed in this paper [13].

It can be seen from Fig. 12 that with the increase of harmonic number, the calculation time increases, and the

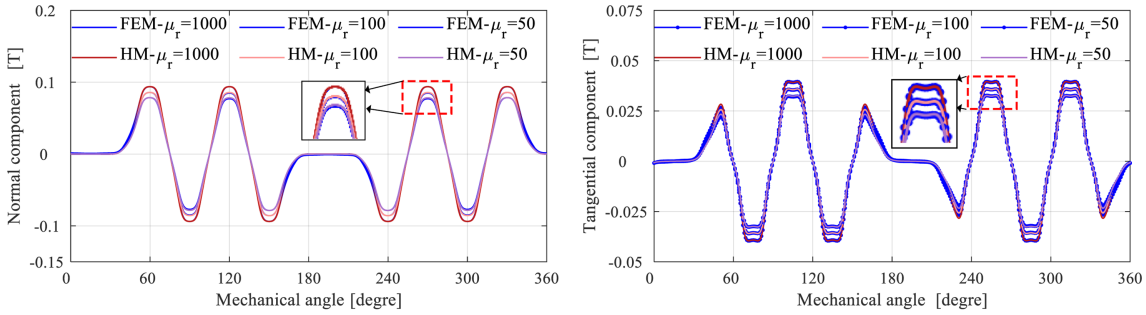

Fig. 10. (Color online) The influence of different relative permeability of Model A. (a) Comparison of the normal component, (b) Comparison of the tangential component.

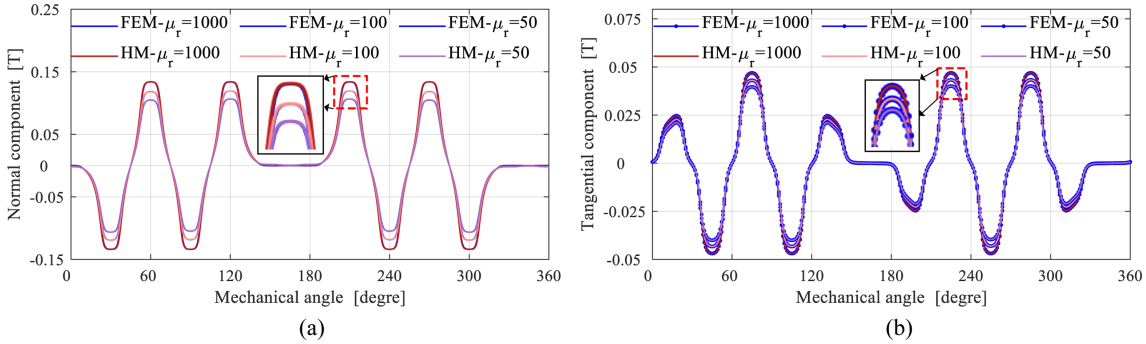

Fig. 11. (Color online) The influence of different relative permeability of Model B. (a) Comparison of the normal component, (b) Comparison of the tangential component.

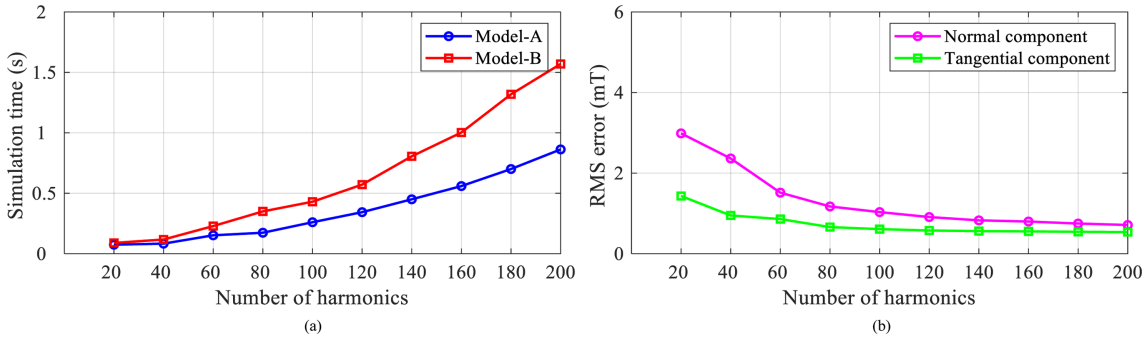

Fig. 12. (Color online) Influence of the number of harmonics. (a) Calculation time, (b) Error of the normal and tangential components of magnetic flux density of Model B.

longer calculation time is not conducive to the initial design of electromagnetic equipment such as motors. When the harmonic number is 120 or 140, the error has met the calculation requirements, and the calculation time cost is small, which is suitable for analyzing complex electromagnetic models. Therefore, selecting the appropriate harmonic number according to the calculation model can reduce the calculation time while ensuring calculation accuracy.

Table 2. The comparison of computation time.

	Model A	Model B
Harmonic Model	1.008 s	1.983 s
FEM	7 s	18 s

$$error = \sqrt{\frac{\sum_{m=1}^{N_{pc}} \left(B_m^{FEA} - B_m^{Ana} \right)^2}{N_{pc}}} \tag{45}$$

The FEM is computationally accurate, and complicated geometric details can be precisely considered. However, it is time-consuming and not conducive to the initial design stages and dynamic analysis optimization. In terms of the computation time, the FEM model has 14638 elements of Model A and 18163 elements of Model B, it requires 7 and 18 seconds to obtain the calculation results [i7-7700 K @ 4.20(GHz) CPU], respectively. The Harmonic Model proposed in this paper, on the other hand, require only 1.008 and 1.983 seconds to get the magnetic calculation results. Therefore, the Harmonic Model is much faster than FEM.

6. Conclusion

This work proposes a general 2D analytical solution for the magnetic field of EE in Cartesian coordinates, based on HM technology. It should be noted that the relative permeability of ferromagnetic materials is embedded into the solution of the static magnetic field, and the nonlinear effect of ferromagnetic materials can be considered by the iterative algorithm. The proposed method can be utilized to analyze various electromagnetic fields including axial flux PM motors and linear PM motors in the 2D Cartesian coordinates system. The correctness of the proposed harmonic model is verified by two numerical examples. The primary advantage of the method is its versatility for magnetic field analysis and offers a new way to quickly and accurately analyze the magnetic field in the 2D Cartesian coordinates system.

Acknowledgment

The authors gratefully acknowledge the support from the National Nature Science Foundation of China (Project Number: 51907027).

References

[1] A. EL-Refaie, IEEE Electrification Magazine **7**, 49 (2019).
[2] T. Rylander, P. Ingelström, and A. Bondeson, Computational Electromagnetics, NY: Springer New York, New York (2013).
[3] J. Dong, Y. Huang, L. Jin, and H. Lin, IEEE Trans. Appl. Supercond. **26**, 1 (2016).
[4] Z. Zhu, Y. Huang, J. Dong, and F. Peng, J. Magn. **24**, 3 (2019).
[5] A. Hemeida and P. Sergeant, IEEE Trans. Magn. **50**, 1 (2014).
[6] M. Aydin and M. Gulec, IEEE Trans. Magn. **52**, 1 (2016).
[7] I. D. Chasiotis and Y. L. Karnavas, Computer Applications in Engineering Education **26**, 749 (2018).
[8] Boughrara, R. Ibtiouen, D. Žarko, O. Touhami, and A. Rezzoug, IEEE Trans. Magn. **46**, 3684 (2010).
[9] D. Zarko, D. Ban, and T. A. Lipo, IEEE Trans. Magn. **45**, 2943 (2009).
[10] T. Lubin, S. Mezani, and A. Rezzoug, IEEE Trans. Magn. **48**, 2080 (2012).
[11] T. Lubin, S. Mezani, and A. Rezzoug, IEEE Trans. Magn. **49**, 5507 (2013).
[12] L. Roubache, K. Boughrara, F. Dubas, and R. Ibtiouen, IEEE Trans. Magn. **54**, 1 (2018).
[13] R. L. J. Sprangers, J. J. H. Paulides, B. L. J. Gysen, and E. A. Lomonova, IEEE Trans. Magn. **52**, 1 (2016).
[14] Z. Djelloul-Khedda, K. Boughrara, F. Dubas, and R. Ibtiouen, IEEE Trans. Magn. **53**, 1 (2017).
[15] Z. Djelloul-Khedda, K. Boughrara, F. Dubas, A. Kechroud, and A. Tikellaline, IEEE Trans. Magn. **55**, 1 (2019).
[16] H. Zhao, C. Liu, Z. Song, and J. Yu, IEEE Trans. Ind. Appl. **57**, 437 (2021).
[17] M. Hajdinjak and D. Miljavec, IEEE Trans. Ind. Electron. **67**, 6721 (2020).
[18] T. Lubin, S. Mezani, and A. Rezzoug, IEEE Transactions on Energy Conversion **27**, 536 (2012).
[19] A. Hemeida and P. Sergeant, IEEE Trans. Magn. **50**, 1 (2014).